arXiv:1303.2704v1 [astro-ph.HE] 11 Mar 2013

Fast Cooling Synchrotron Spectrum as the Origin of GRB Prompt Emission

Z. Lucas Uhm[1,2], Bing Zhang[1,3,2]

ABSTRACT

We show that a fast-cooling synchrotron spectrum has a photon index harder than -1.5, as long as one introduces the evolution of magnetic field in the emission region during the course of emission, an important physical process hitherto ignored in theoretical modeling. By introducing a reasonable decay law of magnetic fields, we model the prompt emission spectrum of GRBs, and found that the low-energy photon index below the injection frequency is typically around -1 in the time scale of seconds, well consistent with the data. The model photon spectrum can be fit with the well-known "Band" function. All these suggest that fast-cooling synchrotron radiation is the dominant mechanism to power GRBs.

Subject headings: gamma-ray burst: general — radiation mechanisms: non-thermal

The radiation mechanism of gamma-ray bursts (GRBs), the most luminous explosions in the universe, remains un-identified after 45 years since their discovery in late 1960s. Synchrotron radiation of electrons accelerated in relativistic shocks has been suggested as the leading mechanism (Mészáros et al. 1994; Daigne & Mochkovitch 1998). Strong magnetic fields in the emission region lead to rapid cooling of electrons (fast cooling). Traditionally it is believed that the fast cooling electrons give rise to a photon spectrum with a power law spectral index -1.5 below the injection frequency (Sari et al. 1998), while observationally the typical low-energy photon spectral index is -1 (Band et al. 1993; Preece et al. 2000; Zhang et al. 2011; Nava et al. 2011). As a result, fast cooling synchrotron mechanism has been disfavored (Ghisellini et al. 2000), and slow cooling due to decay of magnetic field from the shock front (Pe'er & Zhang 2006) or slow heating due to turbulent acceleration (Asano & Terasawa 2009;

---

[1] Kavli Institute for Astronomy and Astrophysics, Peking University, Beijing 100871, China

[2] Department of Physics and Astronomy, University of Nevada Las Vegas, NV 89154, USA; zhang@physics.unlv.edu, uhm@physics.unlv.edu

[3] Department of Astronomy, Peking University, Beijing 100871, China

Murase et al. 2012) have been invoked in order to interpret the GRB spectrum with synchrotron radiation. Other mechanisms were proposed (Rees & Mészáros 2005; Pe'er et al. 2006; Beloborodov 2010; Lazzati et al. 2013; Kumar & Panaitescu 2008), but observations and theoretical arguments suggest that they may not be the dominant mechanism to power the majority of GRBs (Zhang et al. 2012; Vurm et al. 2013; Piran et al. 2009).

A typical GRB prompt emission spectrum is a smoothly connected broken power law called the "Band function" (Band et al. 1993). The high-energy photon spectral index (with a typical value $\beta \sim -2.2$) can be easily interpreted as emission of fast-cooling electrons with an injected power law distribution $Q(\gamma_e) \propto \gamma_e^{-p}$, given a typical injected electron spectral index $p \sim 2.4$. The low-energy photon spectral index (with typical value $\alpha \sim -1$), on the other hand, has defied all known theoretical models. The photosphere model typically predicts $\alpha = +0.4$ (Beloborodov 2010). In order to reproduce the data, some special jet structure has to be introduced (Lundman et al. 2013). For synchrotron radiation, an ironclad value $\alpha = -1.5$ (Sari et al. 1998) has been widely believed in the community.

This well-known index $\alpha = -1.5$ can be derived from a simple argument. Let us consider a continuity equation of electrons in energy space $(\partial/\partial t)(dN_e/d\gamma_e) + (\partial/\partial\gamma_e)\left[\dot{\gamma}_e(dN_e/d\gamma_e)\right] = Q(\gamma_e, t)$, where $dN_e/d\gamma_e$ is the instantaneous electron spectrum of the system at the epoch t, and $Q(\gamma_e, t)$ is the source function above a minimum injection Lorentz factor γ_m of the electrons. For synchrotron radiation, the electron energy loss rate is

$$\dot{\gamma}_e = -\frac{\sigma_T B^2 \gamma_e^2}{6\pi m_e c} \propto -\gamma_e^2 B^2, \tag{1}$$

where σ_T, m_e, and c are Thomson cross section, electron mass, and speed of light, respectively, and B is the strength of magnetic fields in the emission region. For fast cooling, electrons are cooled rapidly to a particular energy $\gamma_c(t)$ (cooling energy) below the injection energy γ_m. In the regime $\gamma_c < \gamma_e < \gamma_m$, one has $Q(\gamma_e, t) = 0$. Also consider a steady state system $(\partial/\partial t = 0)$, then one immediately gets $dN_e/d\gamma_e \propto \gamma_e^{-2}$, i.e. the electron spectral index is $\tilde{p} = 2$. The specific intensity of synchrotron spectrum would have a spectral index $s = (\tilde{p} - 1)/2 = 1/2$ (with the convention $F_\nu \propto \nu^{-s}$) (Rybicki & Lightman 1979). The photon spectral index (defined as $dN_\gamma/dE_\gamma \propto E_\gamma^\alpha$, where E_γ is the photon energy, and N_γ is the photon number flux) would then be $\alpha = -(1 + s) = -1.5$.

The above argument relies on a crucial assumption of a steady state, which is achieved when a constant B is invoked. In a GRB problem, since the ejecta launched from the central engine is expanding in space, the magnetic field strength cannot be preserved as a constant. In the rest frame of a conical jet, flux conservation indicates that the radial (poloidal) magnetic field component decreases as $B_r' \propto r^{-2}$, while the transverse (toroidal) magnetic field component decreases as $B_t' \propto r^{-1}$ (Spruit et al. 2001). As a result, at a large radius from the central engine where γ-rays are radiated, one has a toroidal-dominated magnetic field with $B' \propto r^{-1}$. Here r is the distance from the central engine. Considering other effects (e.g. magnetic dissipation), the decay law may be described by a more general form

$$B'(r) = B'_0 \left(\frac{r}{r_0} \right)^{-b}. \tag{2}$$

We investigate a generic problem of electron fast cooling in a decaying magnetic field delineated by Eq.2, and study the synchrotron emission spectrum. This model does not specify a particular energy dissipation mechanism or particle acceleration mechanism, and hence, can apply to a variety of GRB prompt emission models such as internal shocks (Daigne et al. 2011) and internal collision-induced magnetic reconnection and turbulence (Zhang & Yan 2011). We consider a toy box that contains electrons and a co-moving magnetic field B', which moves relativistically towards the observer with a bulk Lorentz factor Γ. The relativistic electrons are accelerated into a power-law distribution $Q(\gamma_e, t') = Q_0(t')[\gamma_e/\gamma_m(t')]^{-p}$ (for $\gamma_e > \gamma_m(t')$) of a slope p and continuously injected into the box at the injection rate $R_{\rm inj}(t') = \int_{\gamma_m}^{\infty} Q(\gamma_e, t') d\gamma_e$, where t' is the time measured in the co-moving fluid frame. Here $R_{\rm inj}(t')\, \delta t'$ gives the number of electrons injected into the box during the time interval t' and $t' + \delta t'$.

Electrons undergo both radiative and adiabatic cooling. In the rest frame that is comoving with the relativistic ejecta, the evolution of the Lorentz factor γ_e of an electron can be described by (Uhm et al. 2012)

$$\frac{d}{dt'} \left(\frac{1}{\gamma_e} \right) = \frac{\sigma_T}{6\pi m_e c} B'^2 - \frac{1}{3} \left(\frac{1}{\gamma_e} \right) \frac{d \ln n_e}{dt'}. \tag{3}$$

For a conically expanding toy box, we take the comoving electron number density $n_e \propto r^{-2}$, which gives $d \ln n_e = -2 d \ln r$. We divide the injection function $Q(\gamma_e, t')$ into small divisions in time space t' and also in the energy space γ_e, and numerically follow cooling of each group of electrons (between $[t',\, t' + \delta t']$ and $[\gamma_e,\, \gamma_e + \delta\gamma_e]$) individually using Eq.3. We then find the instantaneous global electron spectrum $dN_e/d\gamma_e$ of the system at the current epoch.

We consider four models with different decay indices b in Eq.2. Model [a] takes a constant co-moving magnetic field $B' = B'_0 = 30$ G. This implies that there should be no change in the volume of the box. Thus for this model we drop out the adiabatic cooling term from Eq.3. As shown in Column 1 of Fig.1 and Fig.2, this model gives the familiar electron spectrum $dN_e/d\gamma_e \propto \gamma_e^{-2}$ below γ_m, and the well-known photon spectrum $F_\nu \propto \nu^{-1/2}$ in the fast cooling regime. Model [b] takes $r_0 = 10^{15}$ cm and $b = 1.0$ in Eq.2. This is the case of free conical expansion with flux conservation (no significant magnetic dissipation). As shown in Column 2 of Fig.1 and Fig.2, the electron spectrum and the photon spectrum both harden with time. At 1.0 s after injecting the first group of electrons, the global electron energy spectral index deviates significantly from the $\tilde{p} = 2$ nominal value, and hardens to around $\tilde{p} \sim 1$. The corresponding photon spectrum is nearly flat ($F_\nu \propto \nu^0$), which corresponds to a photon index ~ -1, the typical low-energy photon index observed in most GRBs (Preece et al. 2000; Zhang et al. 2011). This gives a very simple interpretation to the mysterious low-energy photon index, which has challenged theorists for decades. In Columns 3 and 4 of Fig.1 and Fig.2, we present Models [c] and [d], for which a steeper decay index $b = 1.2$ and $b = 1.5$ are adopted, respectively. These cases may mimic the cases when significant magnetic dissipation occurs during the course of synchrotron radiation (Zhang & Yan 2011). As shown in Fig.2, both models also give spectra that are consistent with the observations.

In order to understand the physical origin of such an effect, in Fig.3 we decompose the $t_{\rm obs} = 1.0$ s instantaneous electron spectrum into the contributions of 10 injection time slices, each lasting for 0.1 s. For the constant B' case (Fig.3a), one can see that as the electrons age, they tend to distribute more narrowly in logarithmic energy space, so that the electron number per energy bin increases. This is because in the fast cooling regime, as time elapses, the original electrons with a wide range of energy distribution tend to cool down to a narrow range of cooling energy defined by the ages of the electrons in the group, which are very close to each other at late epochs. Above γ_m, the electron energy distribution remains unchanged with time, since it is always determined by the same injection rate and cooling rate.

The B' decay cases show a more complicated behavior. The distribution of each group of electrons still shrinks as the group ages. However, since at early epochs the magnetic field was stronger, it had a stronger cooling effect so that for a same injection time duration (0.1 s), initially it had a wider spread in energy at a given age (which can be noticed by comparing the 0.1 s electron spectrum for Model [a] and [b] in Fig.1). The later injected electrons are cooled in a weaker B' field, so that their initial spread is narrower. After the same shrinking effect due to cooling pile-up, the groups injected in earlier time slices have a wider electron distribution than the constant B' case. Also the electron spectrum above the injection energy, even though possessing a same spectral index, has a normalization increasing with time due to progressively less cooling in a progressively weaker magnetic field. These complicated effects all work in the direction to harden the spectral index, as seen in Figures 3b, 3c and 3d. For a steeper B'-decay index (e.g. $b = 1.2$ and $b = 1.5$), the late-time injection occurs in an even weaker magnetic field, so that slow cooling is possible. This results in accumulation of electrons around the minimum injection energy γ_m, so that a sharper break in the electron energy distribution is achieved.

The model predicts that the low-energy spectrum below the injection frequency ν_m is curved, due to the complicated cooling effect as delineated in Fig.3. Most GRB detectors have a narrow band pass so that below the peak energy (typically a few hundred keV), there are at most 2 decades in energy. Nonetheless, in the detector band pass, the observed spectra are usually fit by a Band function, with the low energy spectral index $\alpha \sim -1$. Usually time resolved spectral analyses are carried out with a time bin in seconds (Zhang et al. 2011). This is the typical time scale of the slow variability component in most GRB light curves (Gao et al. 2012). We therefore focus on the 1 s and 3 s model spectra. We truncate these spectra in a narrow band (5 keV - 5 MeV) and compare them with the empirical Band function fits (Fig.4). One can observe that most of our model spectra are consistent with the Band function with the correct low-energy spectral indices.

Outside the band pass, our model predicts an asymptotic value of the low-energy electron energy spectral index of $\tilde{p}_a = (6b-4)/(6b-1)$, which is 2/5 for $b = 1$. This is seen in the numerical results of the models (lower panels in Fig.1), and can be derived analytically (see Appendix). According to the simple relationship $s = (\tilde{p}-1)/2$, one gets $s_a = -3/(12b-2)$, which is -0.3 for $b = 1$ (or $F_\nu \propto \nu^{0.3}$). In reality, due to the contribution of the 1/3 segment of the individual electron spectrum, which becomes significant when $\tilde{p}$ approaches 1/3 from above, the asymptotic photon spectrum limit is softened. In this case, it is about -0.2. This corresponds to a photon index of -0.8, which is much harder than the nominal value -1.5. The spectrum is somewhat softer in a narrower band 5 keV - 5 MeV, but is close to -1 (Fig.4).

Our model also predicts that during the very early epochs of a pulse (e.g. the first 0.1 s, 0.01 s, etc), the spectrum should be softer. However, usually there are not enough photons during these early epochs to give a statistically significant spectral analysis. Unusually bright GRBs with distinct pulse structures may be used to test this prediction in the future.

The models presented here are valid when inverse Compton cooling is not important, which requires a highly magnetized ejecta, as has been supported by recent observations (Zhang & Pe'er 2009; Zhang et al. 2011; Yonetoku et al. 2012). The example models presented here only invoke a constant injection function. GRB lightcurves show an erratic behavior, so in reality Q_0 and γ_m should be time-dependent. This would give rise to richer spectral features.

This work is supported by Kavli Institute for Astronomy and Astrophysics (KIAA), Peking University, China, a Cheung Kong Scholar fellowship, and the National Science Foundation, grant AST-0908362. We thank Zhuo Li, Gabriele Ghisellini, and Asaf Pe'er for helpful discussion.

A. Asymptotic Low Energy Shape of Electron Spectrum

The asymptotic low-energy spectral index can be derived analytically for Eq.3. For prompt GRB emission, it is reasonable to adopt a constant Lorentz factor Γ, so that one has $r = c\,t'\Gamma$. We first solve a simpler equation by dropping out the adiabatic term, i.e.

$$\frac{d}{dt'}\left(\frac{1}{\gamma_e}\right) = a\,t'^{-2b}, \tag{A1}$$

where

$$a \equiv \frac{\sigma_T}{6\pi m_e c}\,B_0^2\,(c\Gamma/r_0)^{-2b}. \tag{A2}$$

We then find the solution of electron Lorentz factor at any time t'_j ($> t'_i$)

$$\gamma_e(t'_j) = \left[\frac{1}{\gamma_e(t'_i)} + \frac{a}{1-2b}\left\{{t'_j}^{1-2b} - {t'_i}^{1-2b}\right\}\right]^{-1}, \tag{A3}$$

where $\gamma_e(t'_i)$ is the electron Lorentz factor at an initial time t'_i. For $b > 1/2$, $t'_j \gg t'_i$, and $\gamma_e(t'_j) \ll \gamma_e(t'_i)$, this solution gives $\gamma_e(t'_j) \propto {t'_i}^{2b-1}$. We then get

$$\delta\gamma_e(t'_j) \propto {t'_i}^{2b-2}\,\delta t'_i \propto \left[\gamma_e(t'_j)\right]^{\frac{2b-2}{2b-1}}\,\delta t'_i. \tag{A4}$$

For a constant injection rate $R_{\rm inj}$, we have $\delta N_e \propto \delta t'_i$. Thus, we have an asymptotic behavior of the global electron spectrum as follows.

$$\frac{\delta N_e}{\delta\gamma_e(t'_j)} \propto \left[\gamma_e(t'_j)\right]^{-\frac{2b-2}{2b-1}}. \tag{A5}$$

Now we consider the full Eq.3 that includes the adiabatic term. For $B(r) = B_0\,(r/r_0)^{-b}$ and $r = c\,t'\Gamma$, Equation 3 can be written as

$$\frac{d}{dt'}\left(\frac{1}{\gamma_e}\right) = a\,t'^{-2b} + \frac{2}{3t'}\left(\frac{1}{\gamma_e}\right). \tag{A6}$$

This equation has an analytic solution

$$\gamma_e(t') = t'^{-2/3}\left[\frac{3a}{1-6b}\,t'^{(1-6b)/3} + C\right]^{-1}, \tag{A7}$$

where C is the integration constant of the differential equation, to be determined by the initial condition; $\gamma_e(t'_i)$ at time t'_i. The electron's Lorentz factor $\gamma_e(t'_j)$ at a later time t'_j is found to be

$$\gamma_e(t'_j) = {t'_j}^{-2/3}\left[\frac{{t'_i}^{-2/3}}{\gamma_e(t'_i)} + \frac{3a}{1-6b}\left\{{t'_j}^{(1-6b)/3} - {t'_i}^{(1-6b)/3}\right\}\right]^{-1}. \tag{A8}$$

For $b > 1/6$, $t'_j \gg t'_i$, and ${t'_j}^{2/3}\gamma_e(t'_j) \ll {t'_i}^{2/3}\gamma_e(t'_i)$, this solution gives $\gamma_e(t'_j) \propto {t'_j}^{-2/3}\,{t'_i}^{(6b-1)/3}$. A variation in $\gamma_e(t'_j)$ results only from $\delta t'_i$ for the instantaneous (i.e., at a fixed time t'_j) global electron spectrum; $\delta\gamma_e(t'_j) \propto {t'_j}^{-2/3}\,{t'_i}^{(6b-4)/3}\,\delta t'_i$. This gives the asymptotic behavior of the global electron spectrum

$$\frac{\delta N_e}{\delta\gamma_e(t'_j)} \propto {t'_j}^{\frac{2}{6b-1}} \left[\gamma_e(t'_j)\right]^{-\frac{6b-4}{6b-1}} , \tag{A9}$$

where we have again assumed a constant injection rate $R_{\rm inj}$. Therefore we have the asymptotic low-energy electron spectral index $\tilde{p}_a = (6b-4)/(6b-1)$.

REFERENCES

Asano, K., & Terasawa, T. 2009, ApJ, 705, 1714

Band, D., Matteson, J., Ford, L., et al. 1993, ApJ, 413, 281

Beloborodov, A. M. 2010, MNRAS, 407, 1033

Daigne, F., Bošnjak, Ž., & Dubus, G. 2011, A&A, 526, A110

Daigne, F., & Mochkovitch, R. 1998, MNRAS, 296, 275

Gao, H., Zhang, B.-B., & Zhang, B. 2012, ApJ, 748, 134

Ghisellini, G., Celotti, A., & Lazzati, D. 2000, MNRAS, 313, L1

Kumar, P., & Panaitescu, A. 2008, MNRAS, 391, L19

Lazzati, D., Morsony, B. J., Margutti, R., & Begelman, M. C. 2013, ApJ, 765, 103

Lundman, C., Pe'er, A., & Ryde, F. 2013, MNRAS, 428, 2430

Mészáros, P., Rees, M. J., & Papathanassiou, H. 1994, ApJ, 432, 181

Murase, K., Asano, K., Terasawa, T., & Mészáros, P. 2012, ApJ, 746, 164

Nava, L., Ghirlanda, G., Ghisellini, G., & Celotti, A. 2011, A&A, 530, A21

Pe'er, A., Mészáros, P., & Rees, M. J. 2006, ApJ, 642, 995

Pe'er, A., & Zhang, B. 2006, ApJ, 653, 454

Piran, T., Sari, R., & Zou, Y.-C. 2009, MNRAS, 393, 1107

Preece, R. D., Briggs, M. S., Mallozzi, R. S., et al. 2000, ApJS, 126, 19

Rees, M. J., & Mészáros, P. 2005, ApJ, 628, 847

Rybicki, G. B., & Lightman, A. P. 1979, Radiative processes in astrophysics (New York, Wiley-Interscience, 1979. 393 p.)

Sari, R., Piran, T., & Narayan, R. 1998, ApJ, 497, L17+

Spruit, H. C., Daigne, F., & Drenkhahn, G. 2001, A&A, 369, 694

Uhm, Z. L., Zhang, B., Hascoët, R., et al. 2012, ApJ, 761, 147

Vurm, I., Lyubarsky, Y., & Piran, T. 2013, ApJ, 764, 143

Yonetoku, D., Murakami, T., Gunji, S., et al. 2012, ApJ, 758, L1

Zhang, B., Lu, R.-J., Liang, E.-W., & Wu, X.-F. 2012, ApJ, 758, L34

Zhang, B., & Pe'er, A. 2009, ApJ, 700, L65

Zhang, B., & Yan, H. 2011, ApJ, 726, 90

Zhang, B.-B., Zhang, B., Liang, E.-W., et al. 2011, ApJ, 730, 141

This preprint was prepared with the AAS LaTeX macros v5.2.

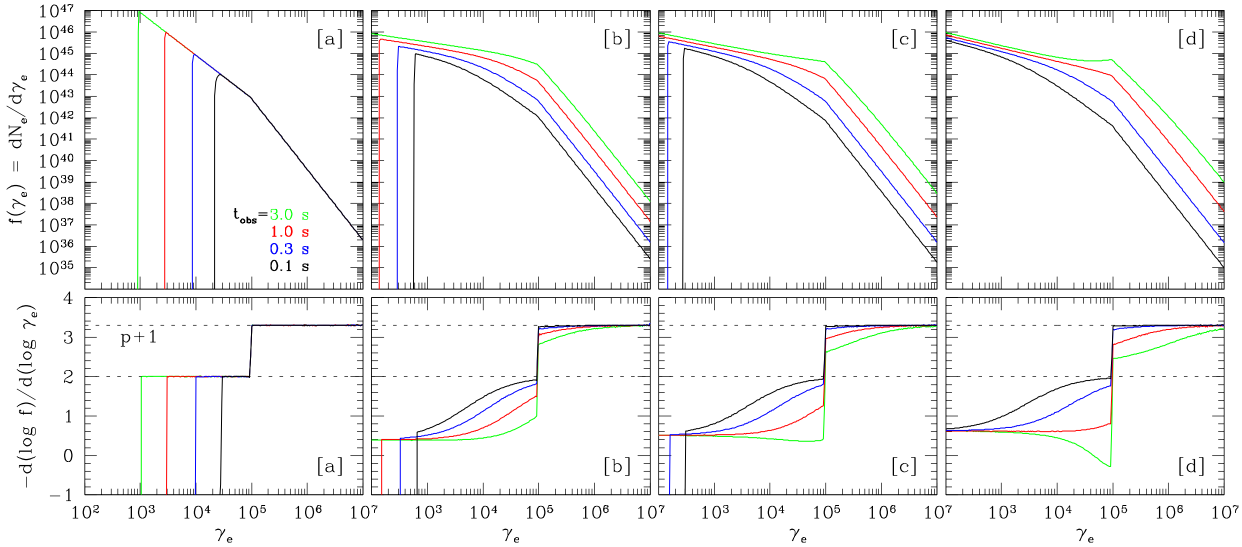

Fig. 1.— The co-moving frame fast cooling electron energy spectrum evolution as a function of time t'. The injected electrons have a power law distribution $Q(\gamma_e, t') = Q_0(t')(\gamma_e/\gamma_m)^{-p}$ above a minimum injection Lorentz factor $\gamma_m = 10^5$, with a power law index $p = 2.3$ for $\gamma_e > \gamma_m$. We take a co-moving magnetic field $B' = B'_0(r/r_0)^{-b}$ with $B'_0 = 30$ G and $r_0 = 10^{15}$ cm. Four models are investigated: [a] $b = 0$; [b] $b = 1$; [c] $b = 1.2$; and [d] $b = 1.5$. For all the models, a constant injection rate $R_{\rm inj} = \int_{\gamma_m}^{\infty} Q(\gamma_e, t')d\gamma_e = 10^{47}\ {\rm s}^{-1}$ is adopted, with both Q_0 and γ_m as constants. The electron injection into the box begins at $r = 10^{14}$ cm. The ejecta is assumed to be moving towards the observer with a Lorentz factor $\Gamma = 300$, and the burst is assumed at a cosmological redshift $z = 1$. For each model, the instantaneous electron spectra at four different epochs since the beginning of electron acceleration are calculated. The four epochs in the observer's frame are: 0.1 s (black), 0.3 s (blue), 1.0 s (red), and 3.0 s (green). For each epoch, the sharp cutoff at low energies corresponds to the "cooling energy" of the system, which is defined by the strength of the magnetic fields and the age of the electrons. Given the same B'_0 field at $r = 10^{15}$ cm, the B' field is stronger at earlier epochs, so that electrons undergo more significant cooling initially. One can see that the cooling energy is systematically lower than that of the constant B' case (Model [a]) as b steepens (Models [b], [c] and [d]). The lower panel of each model shows the local electron spectral index as a function of electron energy γ_e. For Model [a] (constant magnetic field), the electron spectrum shows the well-known broken power law, with the spectral indices $p+1$ and 2 above and below the injection energy, respectively. For other models, even though the index above γ_m remains the same, the index below γ_m is much harder. At later epochs (e.g. 3 s spectra), the index approaches an asymptotic value $\tilde{p}_a = (6b-4)/(6b-1)$.

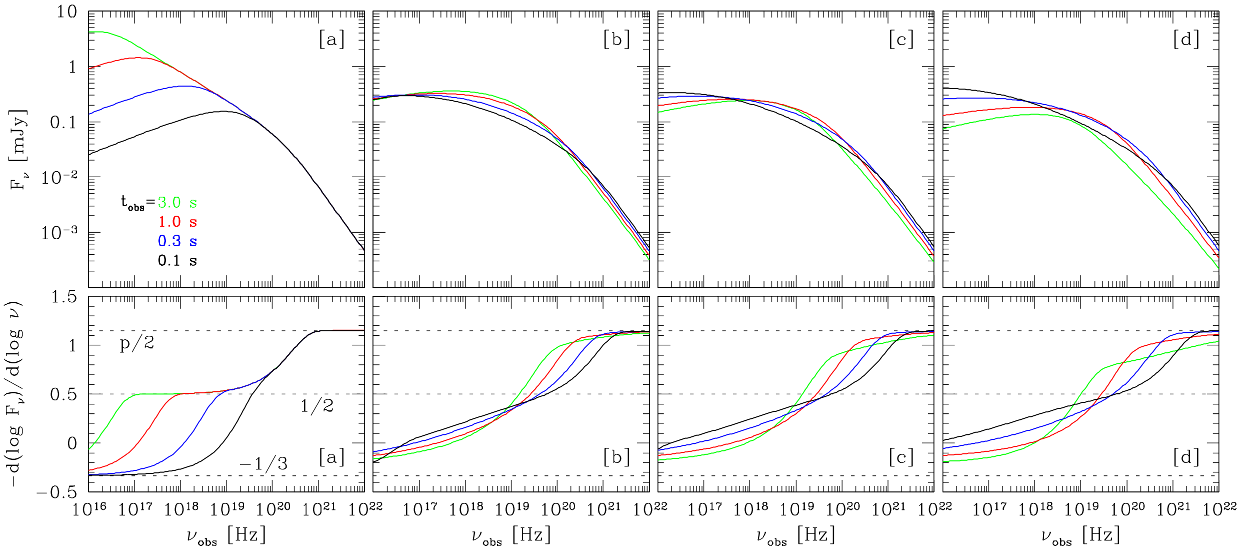

Fig. 2.— The synchrotron emission spectra of electrons with energy distribution presented in Fig.1. The full synchrotron spectrum of each electron (Rybicki & Lightman 1979) is taken into account. The observed spectra are calculated by considering the Lorentz blueshift and cosmological redshift. While the constant B' case (Model [a]) gives rise to the familiar $F_\nu \propto \nu^{-1/2}$ spectrum, the decaying B' cases (Models [b], [c] and [d]) all give rise to much harder spectrum below the injection break ν_m. For the spectra in the seconds time scale (1 s - red; 3 s - green), the low-energy spectral index is nearly flat, consistent with the typical observed photon index -1. Lower panels show local spectral slopes as a function of observed frequency.

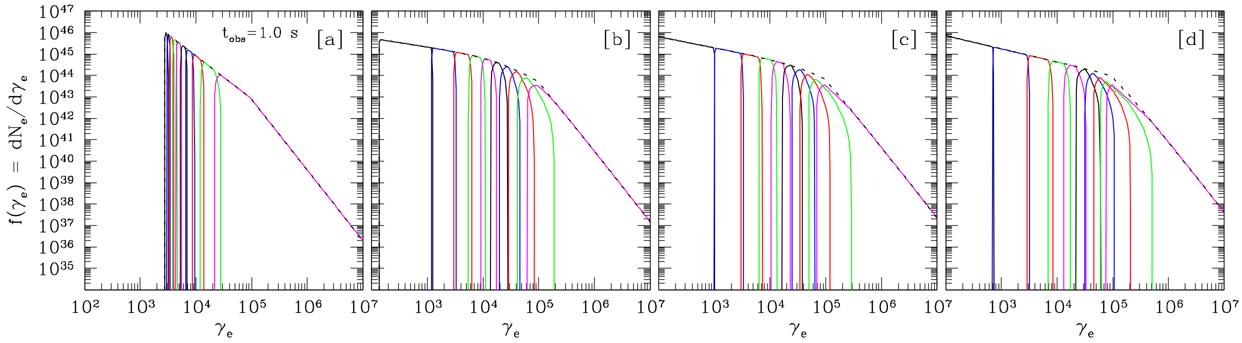

Fig. 3.— Decomposition of electron spectrum at 1 s in the observer's time. In order to see the contributions of electrons injected at different epochs, the electrons are grouped into 10 slices in injection time, each with a duration of 0.1 s. The contributions of each group to the instantaneous electron spectrum at 1 s are marked in different colors. Older groups are cooled down further towards lower energies, so from left to right, curves with different colors denote the electron energy distribution of the electron groups injected from progressively later epochs, with a 0.1 s time step. Dashed curves are the summed total of all electrons.

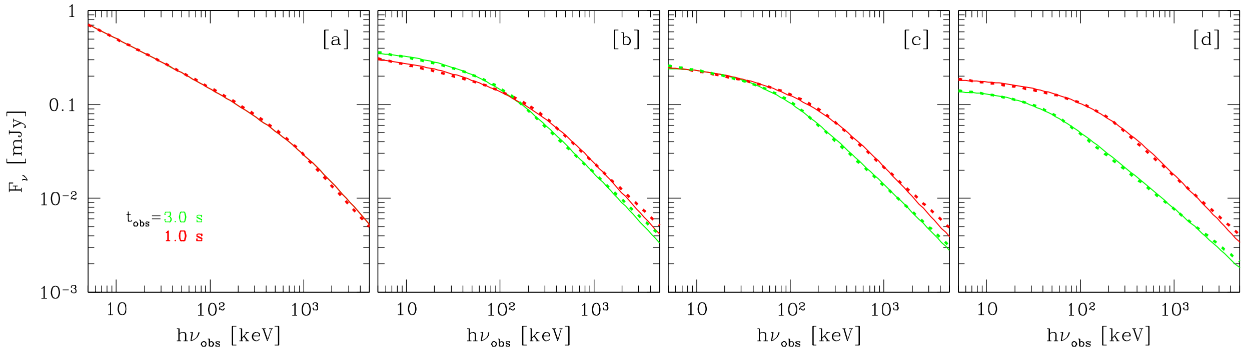

Fig. 4.— A comparison of our 1 s and 3 s model spectra (solid) with the empirical Band function fits (dashed) for all four models in a narrower band pass from 5 keV to 5 MeV. It is seen that the model spectra can mimic the Band function spectra well. The plotted Band function parameters are the following: Model [a]: $\alpha = -1.5$, $\beta = -2.1$, $E_0 = 1800$ keV for both 1 s and 3 s; Model [b]: $\alpha = -1.2$, $\beta = -1.95$, $E_0 = 480$ keV for 1 s, and $\alpha = -1.15$, $\beta = -1.95$, $E_0 = 220$ keV for 3 s; Model [c]: $\alpha = -1.15$, $\beta = -1.92$, $E_0 = 390$ keV for 1 s, and $\alpha = -1.13$, $\beta = -1.92$, $E_0 = 190$ keV for 3 s; Model [d]: $\alpha = -1.1$, $\beta = -1.9$, $E_0 = 330$ keV for 1 s, and $\alpha = -1.05$, $\beta = -1.8$, $E_0 = 100$ keV for 3 s.